C. M. Sonsino and V. Grubisic**

Multiaxial Fatigue Behaviour of Sintered Steels under Combined In- and Out-of-Phase Bending and Torsion

REFERENCE Sonsino, C. M. and Grubisic, V., **Multiaxial fatigue behaviour of sintered steels under combined in- and out-of-phase bending and torsion,** *Biaxial and Multiaxial Fatigue*, EGF 3 (Edited by M. W. Brown and K. J. Miller), 1989, Mechanical Engineering Publications, London, pp. 335–353.

ABSTRACT This paper discusses the fatigue behaviour of sintered steels under multiaxial loading. These steels are the Fe–1.5% Cu and the Fe–2.0% Cu–2.5% Ni, sintered at low and high temperatures, in the densities 7.1 and 7.4 g/cm^3, which are used in the production of several ready-to-assemble automotive parts.

Fully reversed or pulsating combined loading with constant frequency and amplitudes acting in- and out-of-phase, was applied to round notched specimens ($K_{tb} = 1.49$, $K_{tt} = 1.24$) in the finite fatigue life region ($10^4 < N_f < 2 \cdot 10^6$).

The mechanics of crack initiation and propagation as well as rupture were studied using fractography and microfractography. These analyses led to a mechanical model based on local normal stresses for the fatigue life evaluation.

The fatigue life evaluation on the base of the local bending stress obtained under uniaxial loading describes the test results for in-phase combined bending and torsion satisfactorily. But the increase of fatigue strength and life by out-of-phase loading is overestimated in the case of fully reversed loading. However, for design purposes the out-of-phase loading can be neglected because of its beneficial effect in increasing fatigue life for this type of material.

Introduction

Powder metallurgy is a technique which, in comparison to other competing production techniques, such as casting or forging, may offer economic and technical benefits. In order to take advantage of sintering techniques in the design of critical fatigue parts, not only a knowledge of the operational loading is required but also the fatigue behaviour of the respective material under complex loading.

This paper analyses the multiaxial fatigue behaviour of the sintered steels Fe–2.0% Cu and Fe–2.0% Cu–2.5% Ni, sintered at low and high temperatures, in the densities 7.1 and 7.4 g/cm^3, which are used in the production of several ready-to-assemble automotive parts. It aims to enable the design engineer to evaluate multiaxial stress states in high-stressed areas of parts due to geometrical discontinuities like notches or due to a multiaxial external loading. The mechanics of crack initiation as well as rupture are investigated, and a failure hypothesis based on a mechanical model is presented, which allows the proper design of multiaxially loaded parts being manufactured from these materials.

* Fraunhofer-Institut für Betriebsfestigkeit (LBF), Darmstadt, FRG.

Before presenting the results of this investigation, a short overview of the most important features of sintered steels, with regard to manufacturing and strength behaviour, is given.

Notation

Stresses

σ_n	Nominal stress
σ_a	Stress amplitude
σ_m	Mean stress
σ_x, σ_y	Local axial and circumferential normal stresses
τ_{xy}	Local shear stress
σ_1, σ_2	Local principal stresses
σ_{eq}	Local equivalent stress
$\sigma_n(\varphi)$	Local normal stress on an interference plane
$\tau_n(\varphi)$	Local shear stress on an interference plane
$\sigma_{x,a,pure}$	Local normal stress amplitude under pure bending
$\sigma_{x,a,comb.}$	Local normal stress amplitude under combined loading
$\sigma_{x,a,sup.}$	Local supportable stress amplitude
R_m	Tensile stress
$R_{p0.2}$	0.2 per cent yield stress

Other symbols

α	Direction of principal stresses
φ	Inclination of an interference plane
δ	Phase angle
ω	Angular frequency
f	Frequency
t	Time
N_c	Cycles to crack initiation
N_f	Cycles to final rupture
S_τ	Ratio $\tau_{xy,a}/\sigma_{x,a}$
R	Stress ratio $\sigma_{min}/\sigma_{max}, \tau_{min}/\tau_{max}$
P_s	Probability of survival
da/dN	Crack propagation rate
ΔK	Stress intensity
K_t, K_{tb}, K_{tt}	Notch factor, bending, torsion
S_1, S_2	Sintering temperatures
P_1, P_2	Pressure
ϱ	Density

Short overview of manufacturing and fatigue properties of sintered steels

Production parameters

Figure 1(a) shows the steps for manufacturing PM-parts (1). After mixing the powder with other alloying elements the mix is compacted in a specified form

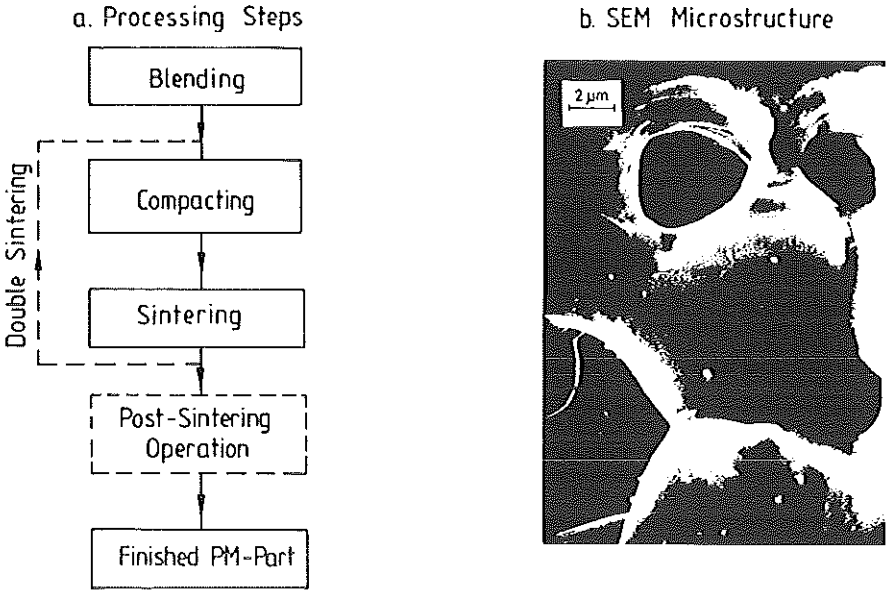

Fig 1 Processing steps for manufacture of PM-parts and microstructure of a sintered steel

and then sintered (single sintering technique) under a protecting and oxide-reducing atmosphere. Due to diffusion during the sintering process the final required strength is reached. To obtain higher densities than 7.2 g/cm^3, and so a higher strength, the compaction and sintering can be repeated. By this technique, called double sintering, densities up to 7.5 g/cm^3 may be attained. Generally, after sintering, a ready-to-assemble part is manufactured. But in many cases a post-sintering operation, such as sizing, carbonitriding, shot peening (**2**)(**3**), or machining can be performed. Figure 1(b) shows the microstructure of a sintered steel; the porosity is the most typical and important feature of such steels. It can be reduced by increased compaction (Fig. 2). But densities above 7.5 g/cm^3 can be obtained only by powder forging.

For sintered steels, in addition to the material parameters, i.e., the alloy composition, it is the density and the sintering temperature which are the decisive production parameters, determining the strength and toughness (**1**)–(**6**). Density has the greatest influence. The choice of material, density and temperature depends on criteria such as required strength, compressibility of the powders, tool wear, and, above all, the economics of the finished product.

Fatigue strength under uniaxial loading

As can be seen from Fig. 3, in the unnotched condition the fatigue strength of sintered steels is lower when compared to structural and tempered steels and, in some cases, when compared to nodular cast iron. However, since components usually exhibit local increases of stress due to geometrical discontinuities,

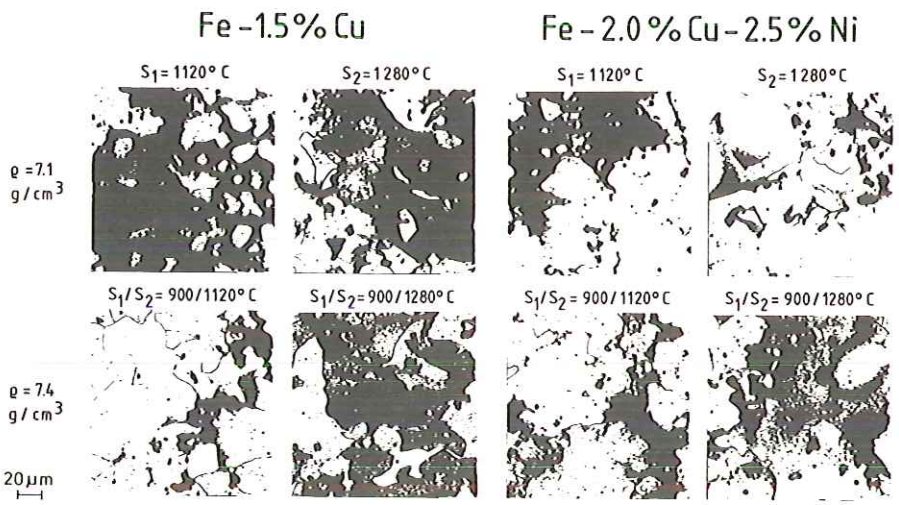

Fig 2 Microstructures

an application-oriented comparison between different materials should be made for the notched condition. Figure 3 shows that the endurance limit data are largely comparable for notched specimens with notch factors, K_t, above 2 and densities above 7.1 g/cm^3. Many sintered components which were previously made from structural, case-hardened or tempered steels lie within this notch factor range (5).

The reason for the comparability of the endurance limit data is the lower notch sensitivity of sintered steels, giving a smaller reduction in fatigue strength with increasing notch factor (5)–(7). The lower notch sensitivity of sintered steels is based on the influence of the pores delaying crack propagation in the region of low stress intensities, see Fig. 4. In this region the rate of crack propagation of sintered steels with densities up to 7.2 g/cm^3 is comparable with those of structural steels and nodular cast iron; in the case of sintered steels of higher density it is even lower and becomes comparable with the data of tempered steels (5)–(7).

Figures 3 and 4 also show that the same fatigue and crack propagation behaviour was established for various alloy types with comparable density and within existing scatter. The reason for this is that these data are determined primarily by processes at pore edges. But static data indicate a significant influence of alloy composition.

Further strength-enhancing measures

In addition to the production influences of density and sintering temperature, there are further possibilities for enhancing the fatigue behaviour. These

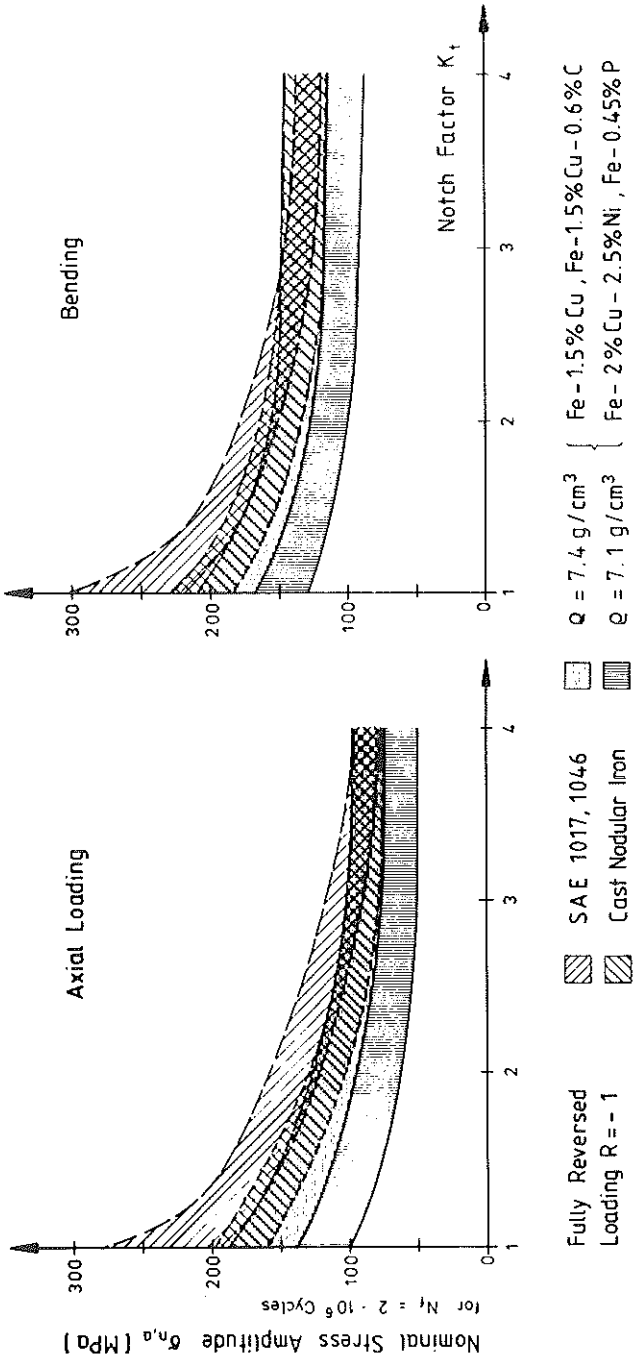

Fig 3 Endurance limit of sintered steels and comparison with wrought and cast materials

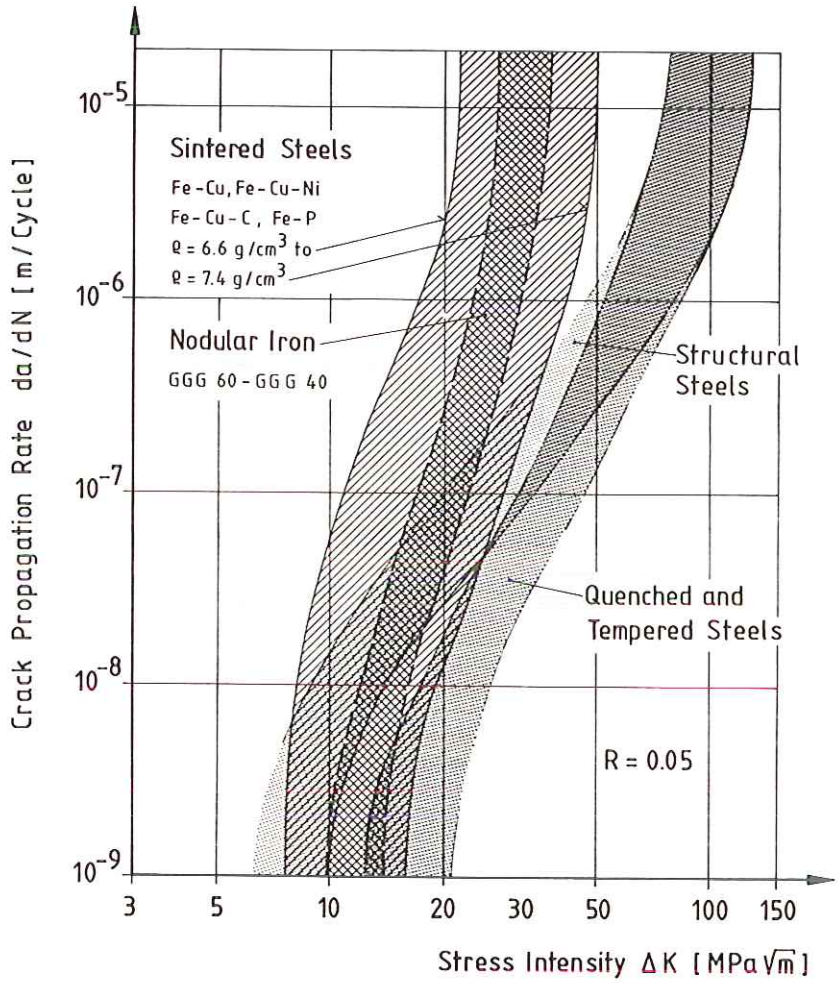

Fig 4 Crack propagation rate and stress intensity for different materials

possibilities include mechanical surface strengthening, such as rolling or coining, which can be carried out in a final sizing operation. By means of these processes it is possible to obtain an increase in the endurance limit of about 35 per cent (5)(8). Even machining performed under a specific surface pressure (due to the reduction of surface porosity and the build up of favourable compressive residual stresses) leads to an improvement in fatigue behaviour as compared to the sintered and non-treated surface condition. Furthermore, increased strength and resistance-to-wear can be achieved by tempering or carbonitriding. For notched components carbonitriding is to be recommended since, in addition to increased hardness, compressive residual stresses are increased (5).

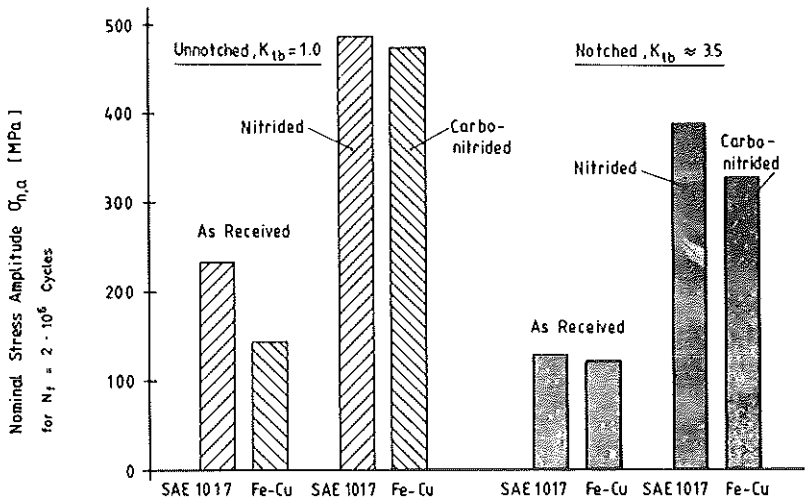

Materials: SAE 1017, normalized, Fe-1.5% Cu, $\varsigma = 7.1 g/cm^3$, $S_1 = 1120°C$, Fully Reversed Bending $R = -1$, $P_s = 50\%$

Fig 5 Endurance limit of wrought steel SAE1017 and of sintered steel Fe–Cu for different heat treatments

Figure 5 shows a comparison between the case-hardened steel SAE 1017 and the Fe–Cu alloy in the untreated and the heat-treated condition. Carbonitriding provides a considerable increase in endurance limit which is comparable to the nitrided steel. For the sintered steel, a higher density would provide higher endurance limit values. Since the increase in the endurance limit through heat treatment is also dependent on the geometry of the specimen, geometrical influences regarding stress gradients must also be taken into account when applying the results to components.

Selection of a valid failure hypothesis

The selection of a valid failure hypothesis has to consider the mechanics of damage initiation and propagation. In the case of ductile materials the damage is initiated primarily by shear stresses and in brittle materials through normal stresses. To calculate the equivalent stress for *ductile materials* the *distortion energy hypothesis* due to von Mises

$$\sigma_{eq} = \sqrt{(\sigma_x^2 + \sigma_y^2 - \sigma_x \cdot \sigma_y + 3 \cdot \tau_{xy}^2)} \quad (1)$$

or the *shear stress hypothesis* due to Tresca, which is similar to the von Mises' hypothesis

$$\sigma_{eq} = \sqrt{\{(\sigma_x - \sigma_y)^2 + 4 \cdot \tau_{xy}^2\}} \quad (2)$$

and for *brittle materials* the *normal stress hypothesis*, also called the principal stress hypothesis

$$\sigma_{eq} = \sigma_{1,2} = \frac{\sigma_x + \sigma_y}{2} \pm \sqrt{\left\{\frac{(\sigma_x - \sigma_y)^2}{4} + \tau_{xy}^2\right\}} \tag{3}$$

are recommended (**9**). Figure 6 shows that under either static or dynamic torsion, the position of the fracture plane depends on the sensitivity of the material to shear or normal stresses, or their combination. The position of the fracture plane indicates the cause of failure and, consequently, a valid hypothesis can be deduced. But as these hypotheses were originally developed for static loading, their application to fatigue is questionable. An evaluation of a multiaxial stress state, for example, with changing directions of principal stresses ($\sigma_{1,2}$)

$$\operatorname{tg} 2\alpha = \frac{2 \cdot \tau_{xy}}{\sigma_x - \sigma_y} \tag{4}$$

fails for ductile materials when the distortion energy hypothesis or the shear stress hypothesis is applied, because the equivalent stress due to both hypotheses is a scalar value and an interaction of deformations in different directions of the material is not considered (**10**)(**11**). Therefore, in recent years, several modifications to failure hypotheses for the evaluation of the fatigue behaviour of ductile materials under multiaxial loading have been developed (**12**)(**13**), covering only special loading cases; a general failure hypothesis for ductile materials is still missing (**12**).

For non-ductile materials the application of the principal stress hypothesis in order to evaluate a multiaxial stress state presents no major problems. As

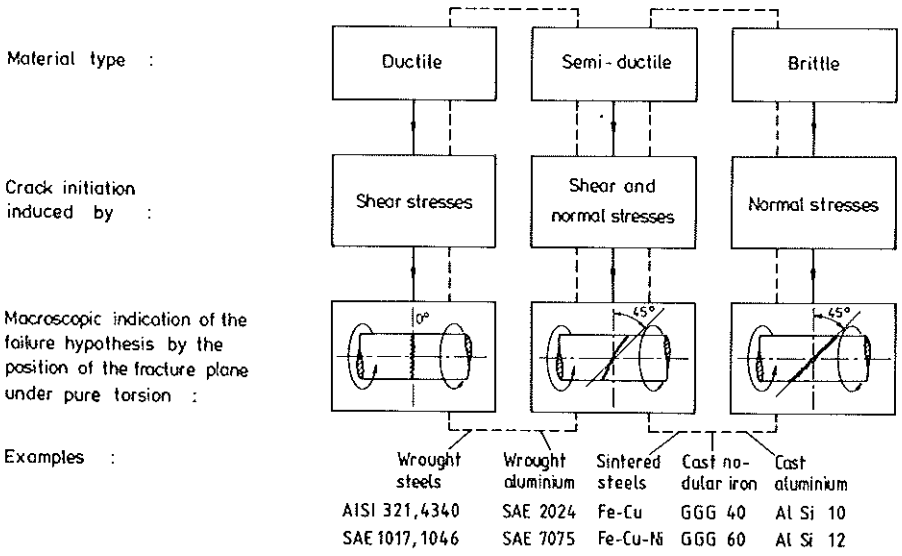

Fig 6 Classification of materials and causes of damage

sintered steels fall into the category between semi-ductile and brittle materials (see Fig. 6) the principal stress hypothesis can be applied to derive an equivalent stress under multiaxial loading. However, the hypothesis must be developed to differentiate between the effects of mean stresses and the stress amplitudes on fatigue life, and also their influence in selecting the critical fracture plane (**14**).

The results discussed in this paper are a part of an extensive investigation carried out with the sintered materials introduced in Tables 1 and 2 (**15**).

Materials and test series

Microstructure and test specimens

Tables 1 and 2 detail the materials studied, their manufacturing parameters, and their static data. The higher sintering temperature leads to a more homogenous material (see Fig. 2) and to better material properties than the lower sintering temperature (**4**). The ferritic Fe–Cu alloy sintered at 1120°C contains Cu-rich zones along the grain boundaries and almost no copper within the grains. After sintering at 1280°C, homogenous Fe–Cu solid solutions are formed and the grain size is increased. For Fe–Cu–Ni the microstructures are similar with the exception that Ni–martensite is formed where the nickel concentration is high. The degree of homogenization is similar, but the grain

Table 1 Material and sintering parameters

Material		*Powder*	P_1 (*MPa*)	S_1 (°C)	P_2 (*MPa*)	S_2 (°C)	ϱ (g/cm^3) (±0.05)
Fe–1.5% Cu	1	WPL 200 + 1.5% Cu	530	1120	–	–	7.1
	2	WPL 200 + 1.5% Cu	500	1280	–	–	7.1
	3	WPL 200 + 1.5% Cu	550	900	550	1120	7.4
	4	WPL 200 + 1.5% Cu	550	900	500	1280	7.4
Fe–2.0% Cu–2.5% Ni	5	WPL 200 + 2.0% Cu + 2.5% Ni	500	1120	–	–	7.1
	6	WPL 200 + 2.0% Cu + 2.5% Ni	460	1280	–	–	7.1
	7	WPL 200 + 2.0% Cu + 2.5% Ni	500	900	550	1120	7.4
	8	WPL 200 + 2.0% Cu + 2.5% Ni	500	900	500	1280	7.4

900°C and 1120°C belt furnace, 20 min in cracked ammonia; 1280°C walking beam furnace, 40 min in 70% N_2–30% H_2.

Table 2 Mechanical properties (As-sintered condition)

Material		ϱ (g/cm^3)	E and E_o^m (GPa)	$S_{Y0.2}$ (MPa) Monotonic Tension	$S_{Y0.2}$ (MPa) Monotonic Compression	$S_{Y0.2}$ (MPa) Cyclic Tens./Comp.	S_{UTS} (MPa)	A_5 (%) ($l_o = 25\,mm$)	Z (%) ($A = 80\,mm^2$)	A_V J	Hardness Hb 2.5/62.5
Fe–1.5% Cu	1	7.1	138 –	183	213	235	287	12	13	39	96
	2	7.1	160 164	287	300	350	357	10	9	45	109
	3	7.4	144 183	203	235	250	332	17	21	101	106
	4	7.4	167 184	290	312	350	371	13	16	77	121
Fe–2% Cu–2.5% Ni	5	7.1	140 –	196	249	258	328	9	9	34	100
	6	7.1	149 157	270	312	317	358	10	11	54	115
	7	7.4	155 154	247	293	325	401	12	14	77	115
	8	7.4	165 171	299	325	340	399	10	14	88	123

* E = mechanical measurement.
E_0 = by ultrasonics.

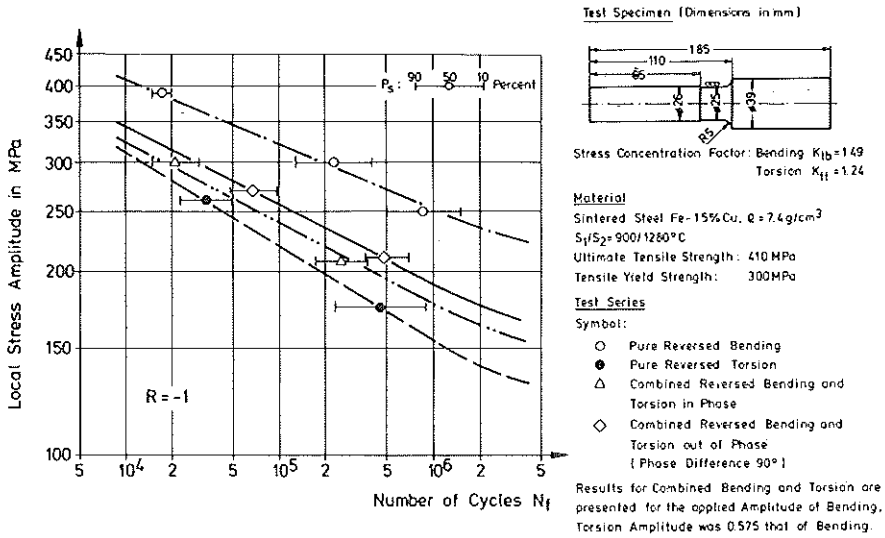

Fig 7 *S–N* **curves for pure and combined bending torsion and tension**

growth, which has been observed in the Fe–Cu alloy, does not occur. The increased sintering temperatures as well as the increase in density also improve the shape of the pores.

For the fatigue tests several fillet notched specimens were isostatically pressed in order to have a homogenous density distribution and no anisotropy effects. After sintering the notches were machined. The shape of the specimens can be seen in Figs 7 and 9. The notch factors for bending $K_{tb} = 1.49$ and for torsion $K_{tt} = 1.24$ were derived by strain measurements in the notch root.

Test conditions

All fatigue tests were carried out with finite fatigue life between 10^4 and $2 \cdot 10^6$ cycles. The tests for the sintered steels were performed under deflection controlled bending and torsion; the local deformation at the notch root was strain controlled at the same time because of deflection control and the constraint of the notch.* The test frequency was 18 Hz. For each material *S–N* curves were obtained, first under constant amplitude pure bending and pure torsion and, subsequently, under combined bending and torsion, being in- and out-of-phase. These load combinations are often observed in service; the simulation of changing principal stress directions is performed by the out-of-

* The stress gradients under bending and the constraint due to the notch caused elastic stresses in the notch root, measured by strain gauges and also calculated using the bending load applied.

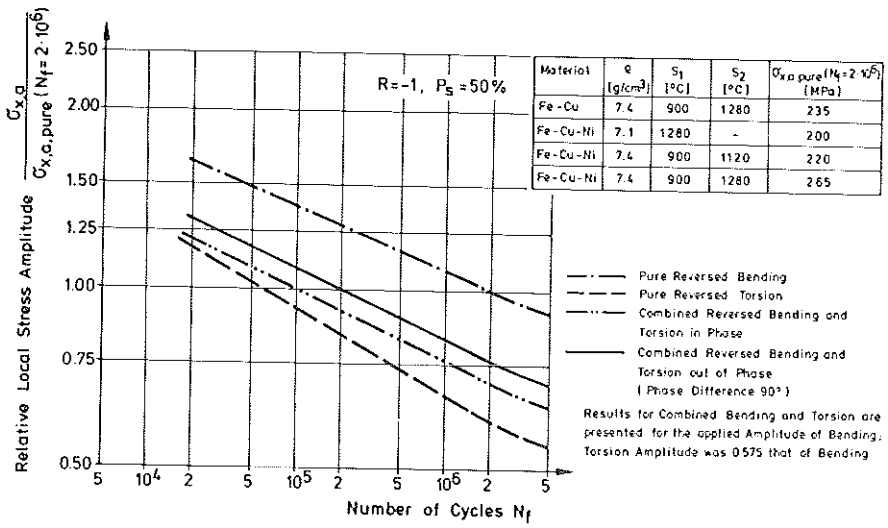

Fig 8 Uniform *S–N* curves for pure and combined bending and torsion for different sintered steels

phase loading. The applied stress tensor on the surface reads

$$\bar{\sigma} = \begin{bmatrix} \sigma_x & \tau_{xy} \\ \tau_{xy} & \sigma_y \end{bmatrix} \tag{5}$$

with the local stress components

$$\sigma_x(t) = \sigma_{x,a} \cdot \sin \omega t \tag{6}$$

$$\sigma_y(t) = A \cdot \sigma_x(t) \tag{7}$$

$$\tau_{xy}(t) = \tau_{xy,a} \cdot \sin (\omega t - \delta) \tag{8}$$

Here A equals 0.215 for the notched specimens. This value was obtained from a strain analysis with the Poisson's ratio $\mu = 0.28$. Under pure bending $\tau_{xy}(t)$ is 0 and $\sigma_x(t)$ is the principal stress, σ_1. In the case of combined in-phase stresses the principal stress is obtained by equation (3). The parameter ω is the angular frequency ($2\pi f$) and δ the phase angle. The applied ratio, $S_t = \tau_{xy,a}/\sigma_{x,a}$ and the stress ratios $R = \sigma_{min}/\sigma_{max}$, τ_{min}/τ_{max}, respectively, are indicated on Figs 7 and 8 as well as on Fig. 13.

Each *S–N* curve was obtained by several tests on at least two stress levels with four to five specimens to enable a statistical evaluation of mean values, with the probability of survival of $P_s = 50$ per cent. The failure criterion for the fatigue tests presented is the fatigue life, N_f, to total rupture of the specimens. Due to the high crack propagation rate of these materials the fatigue life, N_c, to initiate a crack with a defined depth of about 1 mm is about 80 per cent of the total life for the deflection controlled tests.

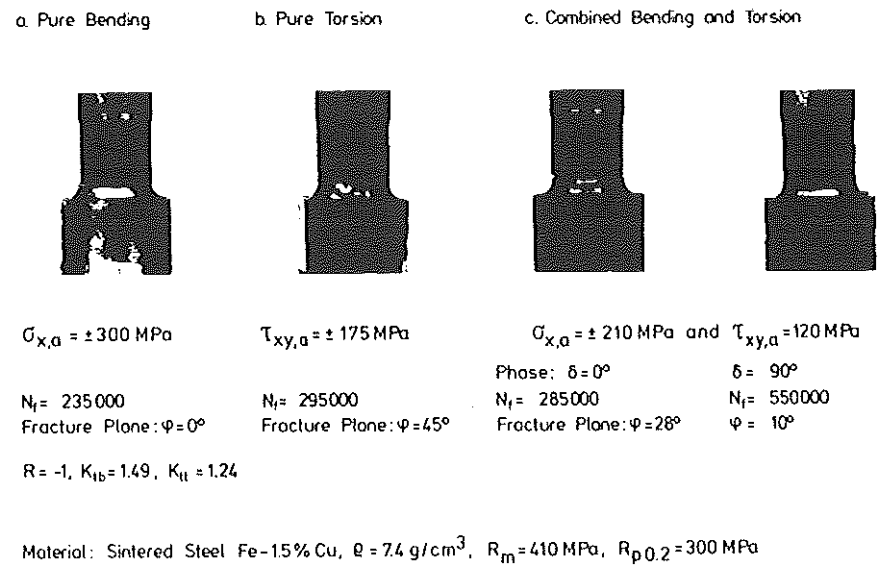

Fig 9 Fracture under pure and combined bending and torsion

Fatigue behaviour and fractographical interpretation of failure mechanisms

Results of fatigue testing

For the curves derived from tests under pure bending and under combined loading the cycles to final rupture N_f are given only in relation to the applied local bending stress amplitude $\sigma_{x,a}$. The cycles to rupture N_f for the tests under pure torsion are given in relation to the applied shear stress amplitude $\tau_{xy,a}$.

In Fig. 7 the results are presented for the high temperature sintered steel Fe–1.5% Cu of density 7.4 g/cm^3. Figure 8 presents the results for all investigated material variants, as the ratio between the S–N curves obtained under different loading modes was similar (**15**). The fatigue strength as well as the fatigue life for the combined multiaxial stresses acting out-of-phase are higher than for the in-phase combined stresses. This behaviour is also observed for cast materials (**14**), indicating that the same basic mechanisms are responsible for both materials, but are different for the ductile steels AISI 321, 4340 or SAE 1017, 1046, for which the fatigue strength is significantly reduced by out-of-phase loading (**10**)(**11**). The fractographical analysis of failures helps to understand the causes of damage.

Fractography

The fracture modes for different loading combinations are presented for the high-temperature sintered steel Fe–1.5% Cu in Fig. 9; the fracture modes for

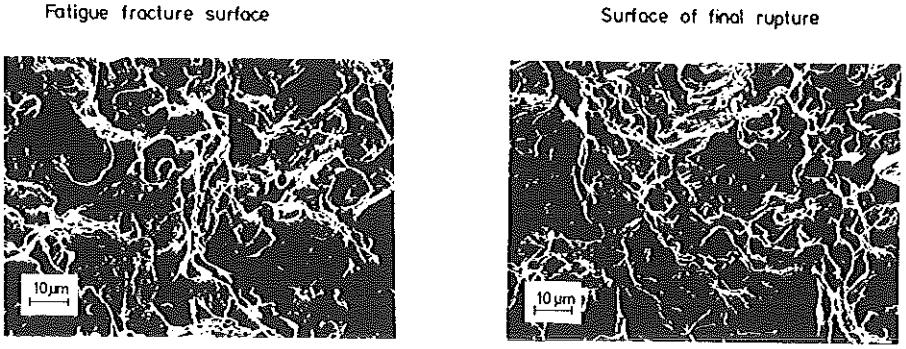

Fig 10 SEM – fractographs for sintered steel. Fe 1.5% Cu; $\rho = 7.4$ g/cm^3

the other sintered variants are identical. Similar macroscopical appearances are also obtained for cast nodular iron and cast aluminium alloys (**14**). It can be seen that the macroscopic inclinations of the fracture planes differ and depend on the loading mode. For pure bending the fracture plane is perpendicular to the specimens axis. This position is independent of the material's ductility. But under pure torsion an inclination of 45 degrees results only for materials where the damaging influence of the normal stresses is primary. In the case of ductile materials the fracture plane under pure torsion is perpendicular to the specimens axis (see Fig. 6). The inclinations of the fracture planes for combined in- and out-of-phase loading will be discussed later.

The microscopic analysis of fatigue fracture surfaces as well as of the surfaces of final rupture, as seen in the scanning electron microscope (Fig. 10), show that for the fatigue failure, as well as for the final rupture, the normal stresses acting perpendicular to the fracture surfaces, are mainly responsible for failure. Cleavage rupture due to normal stresses as in cast iron and cast aluminium alloys is not observed (**14**). In the case of the sintered steel, the final rupture has indeed a ductile appearance (dimpled structure). However, the non-inclined orientation of the dimples indicates no influence of the acting shear stress since no shear dimples (**16**) are present.

Finally, a comparison of the fracture surfaces of specimens which failed under combined loading with fracture surfaces obtained under pure bending or torsion shows nearly identical fractographs, proving the decisive influence of normal stresses for the materials investigated (**15**). This influence is dictated by the microstructure, and Stage I (**16**) crack initiation cannot occur. The stress

raisers due to the microstructural pores cause fatigue damage to take place mainly by Stage II growth, where the crack development is controlled by normal stresses. The crack size during this phase is microscopic. When the crack reachs a technically detectable depth (e.g., 1 mm) the so-called fatigue life to crack initiation, N_c, is reached.

Calculation procedure and evaluation

Analytical model

From the interpretation of the macroscopical and microscopical fracture appearances a calculation procedure based on normal stresses is proposed. The model is given by a surface element, Fig. 11, on which the applied stress components σ_x, σ_y, and τ_{xy} result in a normal stress $\sigma_n(\varphi)$ and $\tau_n(\varphi)$ on an interference plane φ. For the materials investigated the failure is induced by the normal stress

$$\sigma_n(\varphi) = \frac{\sigma_x + \sigma_y}{2} + \frac{\sigma_x - \sigma_y}{2} \cdot \cos 2\varphi + \tau_{xy} \cdot \sin 2\varphi \tag{9}$$

Due to the stress history of the applied stress components for each interference plane φ, a maximum and minimum value of the normal stress $\sigma_n(\varphi)$ is calculated. From these values a normal mean stress and an amplitude are derived

$$\sigma_{n,m}(\varphi) = (\sigma_{n,max} + \sigma_{n,min})/2 \tag{10}$$

$$\sigma_{n,a}(\varphi) = (\sigma_{n,max} - \sigma_{n,min})/2 \tag{11}$$

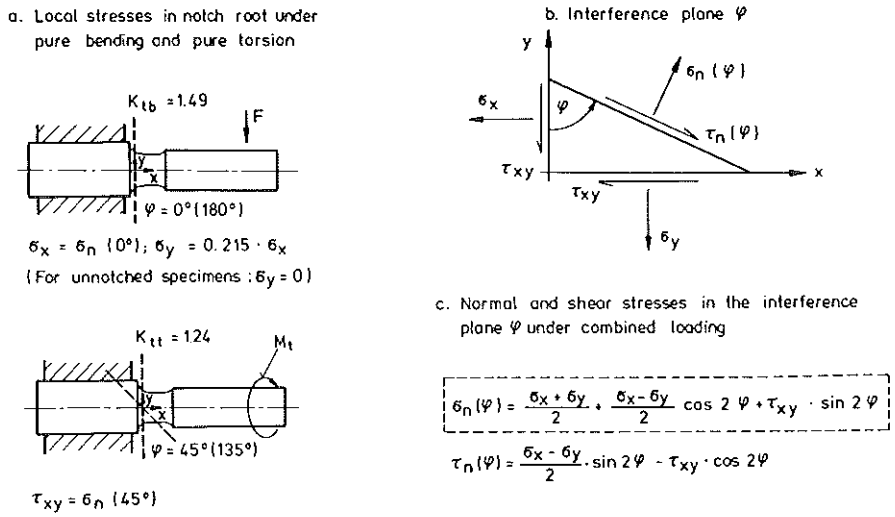

Fig 11 Interference plane and stresses

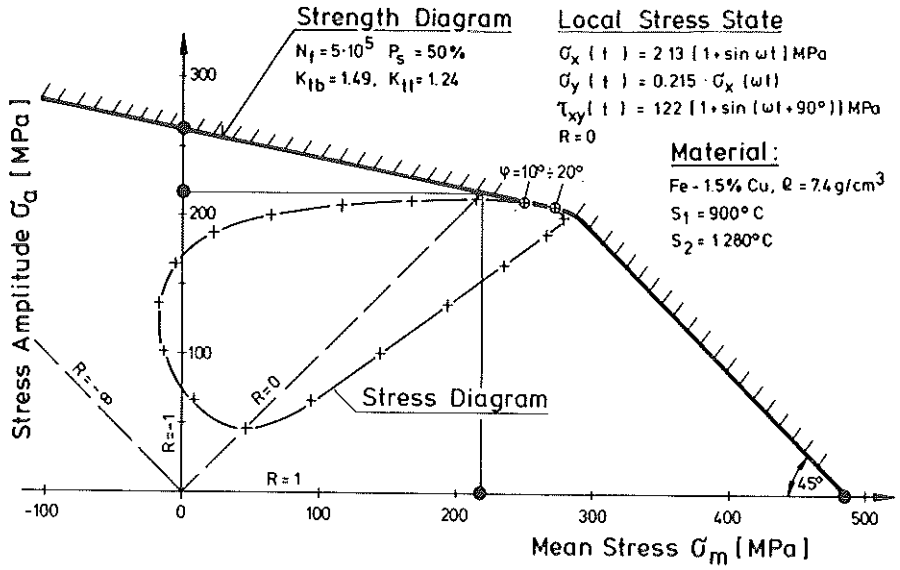

Fig 12 Correlation of the calculated stresses and fatigue strength

The evaluation of the most critical combination of the normal mean stress and normal stress amplitude is carried out by plotting the mean value and amplitude for each plane as a stress diagram (Fig. 12), and then comparing the stress diagram with a strength diagram (Haigh diagram) for a given fatigue life. The strength diagram is derived from test results under uniaxial bending.* The equivalent stress is given by the normal mean stress and amplitude at the interference point. By combination of a strength diagram with the calculated stress diagram, not only the fatigue life is estimated, but also the position of the fracture plane is determined. The inclinations of the fracture planes for combined loading shown in Fig. 9 were calculated by this procedure. Calculated and measured inclinations were nearly identical.

Evaluation of the fatigue tests

The test data for $2 \cdot 10^5$ cycles to rupture are presented in Fig. 13 as values of the ratio between the bending stress under multiaxial and the bending stress under uniaxial stress state via the phase angle. Since the relative difference between the fatigue life to crack initiation, N_c, and the life to final rupture, N_f, within the materials investigated hardly changes, this evaluation is also valid for failure criteria for crack initiation.

* It has to be pointed out that the local supportable stresses under static as well as cyclic bending are higher than properties obtained under axial loading. When notches are present the local values are increased due to the constraint in notch roots.

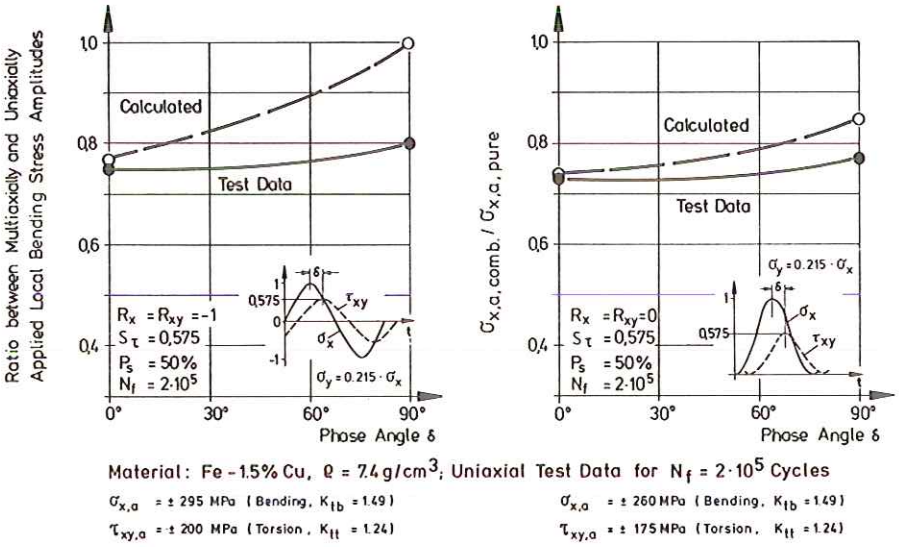

Fig 13 Evaluation of test data for combined bending and shear stresses

The diagram of Fig. 13 shows that, for the high-temperature sintered steel, an increase of the phase angle also increases the fatigue strength for reversed ($R = -1$) and alternating ($R = 0$) loading. The calculation predicts this tendency fairly well, except for the phase angle of 90 degrees and reversed loading, in which case the strength increase is significantly overestimated. Identical results are obtained for all other sintered material variants (**15**), as well as for the cast nodular iron (**14**).

One reason for this discrepancy between the calculation and the test results may be that the influence of torsion is not properly considered. On the other hand, the strength diagram used for the fatigue calculation takes into account only the local bending stresses obtained under uniaxial loading and, therefore, contains only the influence of the stress gradient for bending. But during multiaxial loading the stress gradient for torsion influences the fatigue behaviour too, so that the high-stressed volume in the notch root varies according to the loading mode. The influence of volume size on fatigue life and on the value of the supportable fatigue strength has often been discussed for uniaxial loading (**17**)–(**19**). This aspect obviously plays an important role also in multiaxial fatigue. For that reason it should be given emphasis in future investigations on multiaxial fatigue.

Summary

In this paper the fatigue behaviour of several sintered alloys under multiaxial loading has been presented. The mechanics of crack initiation and propagation

as well as rupture were studied using fractography. These analyses led to a mechanical model based on normal stresses for fatigue life evaluation. Basically, the phase shift between bending and torsion increases the fatigue life of these materials. The calculation of the fatigue life on the basis of the local bending stress obtained under uniaxial loading for in-phase combined bending and torsion corresponds to the experimental results. The increase of fatigue strength by out-of-phase loading is overestimated in the case of fully reversed loading ($R = -1$).

If the phase relation is not known for components manufactured from these materials it is proposed that the case of in-phase loading should be considered as the most critical loading case.

All results were obtained for sintered steels having densities of 7.1 and 7.4 g/cm^3. The same calculation procedure can be applied to sintered steels at lower densities because of their lower ductility levels. However, for sintered materials with higher density and, therefore, higher ductility the influence of shear stresses has to be considered using a different calculation procedure.

Acknowledgements

The authors acknowledge the German Research Community, Bonn, (DFG) for the financial support and Dr G. Schlieper, Sintermetallwerk Krebsöge GmbH, Radevormwald, for the manufacturing of the test specimens. The authors acknowledge also Dr J. Neugebauer for the presentation of this paper during the conference.

References

(1) HIRSCHHORN, J. S. (1969) *Introduction to powder metallurgy*, American Powder Metallurgy Institute, The Colonial Press, Princeton, New Jersey.
(2) ESPER, F. J., SONSINO, C. M., and LEUZE, G. (1984) Design criteria for PM parts submitted to fatigue, Int. Powder Metallurgy Conference, 17–22 June, Toronto.
(3) SONSINO, C. M., SCHLIEPER, G., and HUPPMANN, W. J. (1984) How to improve the fatigue properties of sintered steels by combined mechanical and thermal surface treatments, Int. Powder Metallurgy Conference, 17–22 June, Toronto.
(4) SONSINO, C. M., SCHLIEPER, G., and HUPPMANN, W. J. (1982) Influence of homogeneity on the fatigue properties of sintered steels, Int. Powder Metallurgy Conference, 21–25 June, Florence.
(5) SONSINO, C. M. (1984) Schwingfestigkeit von verschiedenen Sinterstählen und Bemessungskriterien für gesinterte Bauteile, Fraunhofer-Institut für Betriebsfestigkeit (LBF), Darmstadt, Bericht Nr. FB-170.
(6) SONSINO, C. M. (1981) Ermittlung anwendungsrelevanter Kenngrößen für Sintermetalle, Fraunhofer-Institut für Betriebsfestigkeit (LBF), Darmstadt, Bericht Nr. FB-158.
(7) ESPER, F. J., LEUZE, G., and SONSINO, C. M. (1981) Characteristic properties of powder materials relevant to fatigue design, Powder Metallurgy Int., **13**, 203–208.
(8) TAKEYA, Y., HAYASAKA, T., SUZUKI, M., and KAMADA, A. (1982) Surface rolling of sintered gears, Int. Congress and Exposition, Detroit, 22–26 February 1982, SAE Techn. Paper Series No. 82 02 34.
(9) ROS, M. and EICHINGER, A. (1950) Die Bruchgefahr fester Körper bei wiederholter Beanspruchungsermüdung, Eidgenössische Materialprüfanstalt (EMPA), Zürich, Bericht Nr. 173.

(10) GRUBISIC, V. and SIMBÜRGER, A. Fatigue under combined out of phase multiaxial stresses, *Fatigue Testing and Design*, Vol. 2, pp. 27.1–27.28. (See Int. Conference, 5–9 April 1976, The City University, London.)
(11) SONSINO, C. M. and GRUBISIC, V. (1985) Fatigue behaviour of cyclically softening and hardening steels under multiaxial elastic–plastic deformations, *Int. Symposium on Biaxial/Multiaxial Fatigue, ASTM STP 853*, ASTM, Philadelphia, PA, pp. 586–605.
(12) GARUD, Y. S. (1981) Multiaxial fatigue: a survey of the state of the art, *J. Testing Evaluation*, **9**, 165–178.
(13) BROWN, M. W. and MILLER, K. J. (1982) *Two decades of progress in the assessment of multiaxial low-cycle fatigue life, ASTM STP 770*, ASTM, Philadelphia, PA, pp. 482–499.
(14) GRUBISIC, V. and SONSINO, C. M. (1982) Mechanics of fatigue failure of cast alloys and sintered steels under multiaxial loading, International Spring Meeting on Crack Initiation under Complex Loadings, Paris, 22–23 May, 1984.
(15) SONSINO, C. M. (1983) Multiaxial fatigue behaviour of sintered steel under combined in and out of phase biaxial stress states Fraunhofer-Institut für Betriebsfestigkeit (LBF), Darmstadt, Report No. FB-168 (in German).
(16) SCHMITT-THOMAS, K., KLINGELE, H., and WOITSCHEK, A. (1970) Mikromorphologie metallischer Brüche (The Micromorphology of Metallic Fractures), *Prakt. Metallographie*, **7**, 538–560.
(17) SIEBEL, E. and STIELER, M. (1955) Ungleichförmige Spannungsverteilung bei schwingender Beanspruchung, *VDI-Zeitschrift*, **97**, 121–126.
(18) KLOOS, K. H. (1976) Einfluß des Oberflächenzustandes und der Probengröße auf die Schwingfestigkeitseigenschaften, VDI-Bericht Nr. 268, pp. 63–76.
(19) HARIG, H. (1985) Größeneinfluß bei Ermüdungsvorgängen, *Ermüdungsverhalten metallischer Werkstoffe* (Edited by MUNZ, D.), DGM Informationsgesellschaft, Oberursel.